ASTEC - RAVEN coupling for uncertainty analysis of an ingress of coolant event in fusion plants

ASTEC - RAVEN coupling for uncertainty analysis of an Ingress of Coolant Event in fusion plants

Pietro Maccari[a], Mattia Massone[b], Andrea Bersano[c], Fulvio Mascari[b], Antonio Cervone[b], Sandro Manservisi[a].

[a] UNIBO, Industrial Engineering Department (DIN), Via dei Colli 16, 40129, Bologna, Italy
[b] ENEA C.R. Bologna, FSN-SICNUC, Via Martiri di Monte Sole 4, 40129, Bologna, Italy
[c] Politecnico di Torino, Energy Department, Corso Duca degli Abruzzi 24, 10129, Turin, Italy

Corresponding author:
Pietro Maccari: pietro.maccari2@unibo.it
Fulvio Mascari: fulvio.mascari@enea.it

Abstract
The integrated ICE (Ingress-of-Coolant Event) facility, scaled 1/1600 with respect to the ITER-FEAT design, was built at JAERI with the aim of reproducing the phenomenology occurring in an ICE accident. An ICE occurs when a rupture in the coolant pipes causes the pressurized coolant to enter into the Plasma Chamber, which is held under high vacuum condition. A suppression system is used to mitigate the overpressurization and to prevent mechanical damages to the structures. The CPA module of the ASTEC severe accident code (Study carried out with ASTEC V2, IRSN all rights reserved, [2020]), has been adopted for the modeling and the simulation of a test conducted in the ICE facility. The experimental results of the main thermal-hydraulic parameters have been compared to the code results to characterize the ASTEC capability to predict the phenomenology of a low-pressure two-phase flow transient occurring in a fusion reactor. By coupling the ASTEC code with the uncertainty tool RAVEN, developed by Idaho National Laboratory, an uncertainty analysis has been conducted on the transient. The aim of the present activity is to investigate the dispersion and the sensitivity of the code response to the variation of selected uncertain input parameters, which could influence the simulation of an ICE. The activity also provides a first application of uncertainty analysis through the RAVEN-ASTEC coupling.

Keywords: Ingress of Coolant Event; ASTEC; RAVEN; Uncertainty Analysis; High Performance Computing.

1. Introduction

The rupture of the cooling tubes located in the Plasma-Facing Components of a fusion reactor is considered to be one of the most important accident scenarios to be assessed in the safety analyses of a fusion nuclear plant [1]. With the aim of simulating and analyzing the low-pressure thermal-hydraulics of an ICE (Ingress-of-Coolant Event) type accident in a fusion reactor, the ICE test facility was built at JAERI (Japan Atomic Energy Research Institute – Naka Laboratories) [2]. The facility scaling factor is 1/1600 [1][3], with respect to ITER FEAT design [4]. The ingress of coolant fluid in vacuum and high temperature environment, like the Plasma Chamber (PC) of the reactor, leads to the loss of vacuum conditions and pressurization of the PC and the Vacuum Vessel (VV), possibly leading to structural damages. In order to mitigate the over-pressure of the chambers and ensure the integrity of the system, a suppression system is tested in the facility.

In the last years, thermal-hydraulic and Severe Accident (SA) simulation codes, developed for fission reactor safety analyses, have been used in the framework of nuclear fusion reactor safety. Considering this, the capability of these codes to be able to simulate the low-pressure phenomena typical of ICE accident scenario has to be investigated. Previous examples of SA codes application to an ICE accident are reported in [5] for MELCOR and [6] for ASTEC.

In the present work, one of the objectives is the investigation of the ASTEC CPA module [7] capability in fusion safety thermal-hydraulic analyses. Therefore, in order to qualitatively evaluate the performance of the code to reproduce the thermal-hydraulic phenomenology of an ICE, a fast running ASTEC-CPA nodalization of the ICE facility has been realized. The code results of the deterministic sequence simulation have been discussed and compared with the facility experimental results, focusing the attention on the thermal-hydraulic phenomena governing the PC pressurization.

The second part of the paper deals with the description of an Uncertainty Analysis (UA) application to the same test simulation. The analysis has been carried out by coupling the ASTEC code with the UA tool RAVEN [8]. The approach adopted for the UA follows the main methodologies described in the work previously conducted in [9] for the TRACE-DAKOTA coupling. The PC pressure has been chosen as Figure Of Merit (FOM) of the UA. As a result of the statistical analysis, basic statistics have been applied on the FOM and the correlations between the selected uncertain input parameters and the FOM have been evaluated through the use of the Pearson and the Spearman coefficients. The aim of the UA is not to perform an exhaustive uncertainty study, but to provide insights characterizing the dispersion of the results against the available experimental data. Moreover, with this work the authors provide a first example application of UA through the RAVEN-ASTEC coupling developed interface, by employing a High Performance Computer (HPC) for the reduction of the calculation time. The computing resources and the related technical support used for this work have been provided by CRESCO/ENEAGRID High Performance Computing infrastructure and its staff [10].

The research activity has been developed in the framework of a collaboration between ENEA and IRSN on “ASTEC for fusion”.

2. ICE test facility and case-4 experiment description

2.1 ICE facility

The integrated ICE facility [2] was built at JAERI laboratory to characterize the thermal-hydraulic two-phase flow of an ICE in the ITER reactor. Its components scaling factor against the ITER FEAT design is 1/1600. A schematic drawing of the facility is shown in Fig. 1, left. A detailed description can be found in [3] and in [9]. The PC simulates the volume containing the plasma in ITER as a horizontal tank with insulated walls. The VV is a smaller horizontal cylinder located below the PC. The steel walls of the two cylindrical chambers can be heated up by electric heaters. The PC and the VV are connected by a Simulated Divertor (SD) made of a rectangular metal frame with 12 slits, representing the slits of the ITER divertor [3]. Three nozzles connect a pressurized boiler to the PC. High temperature pressurized water can be injected from the boiler to the PC, simulating the rupture of the ITER cooling tubes in an ICE. A Relief Pipe (RP) connects the VV bottom to a vertical Suppression Tank (ST), located under the VV. Along the RP a Magnetic Valve (MV) is set to open at the PC pressure set-point (0.15 MPa), simulating a rupture disk. The ST system is designed to limit the pressure increase in the PC and VV tanks. The RP outlet is immersed under the ST water surface to enhance the steam condensation.

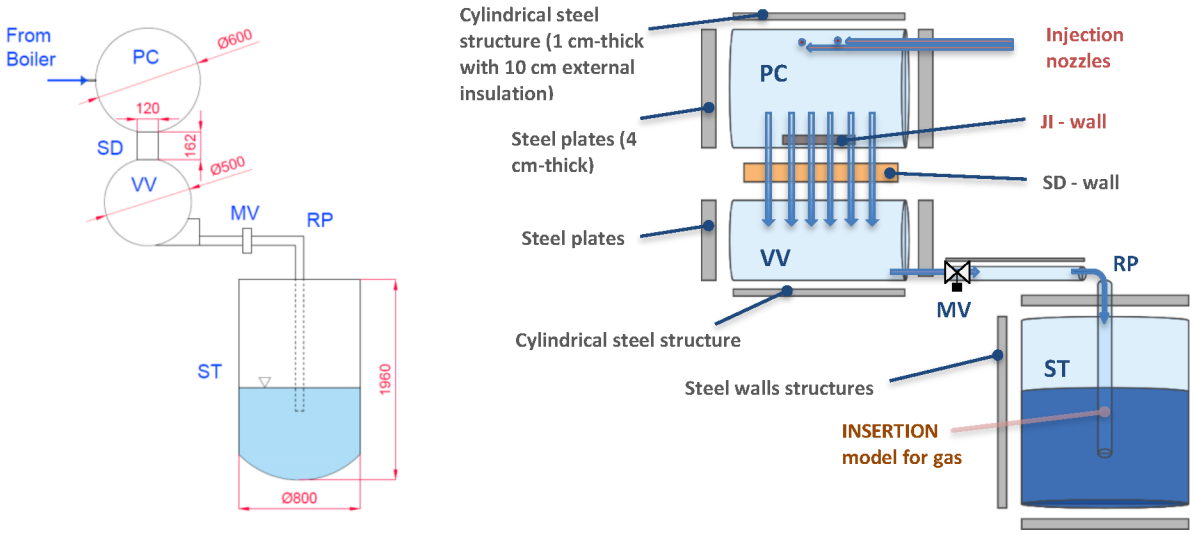

Fig. 1. Schematic view of the integrated ICE facility [9] (left); scheme of the CPA nodalization of the ICE facility (right).

2.2 Case-4 experiment description

The chosen transient for this work is Case-4 of the ICE experimental campaign performed in March 2000 [11]. At the Start Of the Transient (SOT) the PC and VV heaters are turned off and the boiler water injection is performed from 2 out of the 3 PC nozzles for 45 s. Table 1 summarizes the main initial conditions and parameters of the sequence.

Table 1: Initial conditions of the ICE test

Parameter	**Value**
PC, SD, VV initial wall temperature	503.15 K
PC, SD, VV initial pressure	1000.00 Pa
ST initial water and wall temperature	293.15 K
MV opening pressure set point	0.15 MPa
Boiler pressure	2.00 MPa
Water injection duration	45. s
Injected water temperature from boiler	423.15 K

The sequence can be divided into four main Phenomenological Windows (PhWs), as identified in [9]:

- PhW0 (0 – 10 s): Initial phase of the transient without water injection and MV closed. The PhW ends at the beginning of the water injection.
- PhW1 (10 – 55 s): Pressurized water is injected in the PC starting at SOT (t = 10 s). A fast pressurization of the PC and of the VV is caused by the water flashing in the vacuum environment; the heating from the PC walls at higher temperature also contributes to the pressurization. Once the PC pressure set point (0.15 MPa) is reached, the opening of the MV is triggered and the pressurization of the PC and VV is limited by the action of the ST system. Hence, the pressure evolution along the PhW is determined by the weight of the two counteracting phenomena. The PhW ends after 45 s, with the end of the injection.
- PhW2 (55 – 100 s): After the end of the injection, the PC and VV feature a fast depressurization due to the pressure suppression action of the ST. The PhW ends when the PC and VV depressurization is completed.
- PhW3 (100 – 300 s): The PC, VV and ST pressure is almost constant. PC and VV superheated steam temperature increases due to the heat exchanged with the hot surrounding walls.

3. *Description of ASTEC code and ICE facility nodalization*

3.1 Description of the ASTEC code and the CPA module

The ASTEC code [7] (Accident Source Term Evaluation Code), jointly developed until 2015 by the French "Institut de Radioprotection et de Sûreté Nucléaire" (IRSN) and the German "Gesellschaft für Anlagen und Reaktorsicherheit mbH" (GRS) and developed now only by IRSN, aims at simulating an entire Severe Accident (SA) sequence in nuclear water-cooled reactors from the initiating event through the release of radioactive elements out of the containment. It features a modular structure where each module is dedicated to the simulation of a specific set of physical phenomena or related to a specific reactor zone. The main applications of the ASTEC code include source term evaluation studies, Probabilistic Safety Assessment (PSA2), accident management studies, etc. In the present work, the CPA module of ASTEC has been employed for the modelling of the ICE facility and the simulation of the test.

CPA [12] is the ASTEC module, based on mechanistic models, that simulates all the relevant thermal-hydraulic processes and plant states taking place in the containment compartments of a Light Water Reactor (LWR) (e.g. gas distribution, pressure build up, condensation, hydrogen combustion, etc.). The discretization model adopted is a lumped-parameter one, where the compartments are divided into control volumes (zones) whose status is defined by the temperatures and masses of each component. For an adequate simulation of the different systems or boundary conditions, specific junction models are implemented, such as rupture discs, atmospheric valves, suppression systems etc. In CPA the simulation of gas flow and water drainage is strongly separated, and different models are dedicated to each phase.

The CPA module has already been used in the past for simulating low-pressure environments [6], and has been chosen to model the ICE event because of its good behavior in dealing with low pressure thermal-hydraulics.

3.2 Description of the ASTEC (CPA) nodalization of the ICE facility

The nodalization scheme developed to model the ICE facility should be able to assess and qualitatively describe the main low-pressure thermal-hydraulic phenomena occurring in the selected test but without being too complex since the purpose is not to perform detailed deterministic analyses. Limiting the input complexity also helps to reduce the required computational resources, which constitutes a relevant issue when large number of simulations have to be performed, as is usual with uncertainty tools like RAVEN.

The nodalization features one CPA zone for each of the PC, VV and ST. The employed "NONEQUIL" zone type of CPA is able to simulate thermal non-equilibrium condition between the gas and the liquid phases, and so it adopts distinct values for the liquid and the gas temperatures in the volume [12]. Two zones have been employed for the modelling of the RP between the VV and the ST, modeling the vertical and horizontal segments of the pipe. The SD has been modeled as a part of the PC, i.e. its volume belongs to the PC one. In order to follow the CPA best practice, three environment zones are used for the heat losses evaluation: each one has the same elevation of the tank (PC, VV, ST) to which it is thermally coupled. The pressurized boiler is not included in the nodalization, but is modelled as a boundary condition using the experimental data of pressure, temperature and mass flow rate injected in the PC. In Fig 1 (right) a scheme of the ICE nodalization is reported. The PC zone is coupled to a lateral steel structure (cylindrical, 1 cm-thick) with 10 cm of external insulation and two vertical steel plates (4 cm-thick, representing the lateral flanges) without insulation. The same approach is used for the VV chamber external walls modelling. The SD is modelled as a horizontal steel heat structure coupled to the PC through a bottom surface and to the VV through a ceiling surface. The heat structures considered for the ST are: a lateral cylindrical wall, a top and a bottom walls and an internal structure thermally coupled to the RP descending volume. 12 parallel connections are realized for the 12 divertor slits between VV and PC. All wall structures are coupled on their external face with the environment zone located at the same elevation of the corresponding facility zone. The zone related to the horizontal part of the relief pipe is connected to the VV through a valve junction, which models the MV; the latter opens at the PC pressure set point with a selected delay. The RP vertical zone is connected to the ST pool using the "INSERTION" model. It is a dedicated CPA model which is able to predict the behavior of steam and gases injected inside the colder water of the ST pool through an immersed pipe: a fraction of the steam entering the water pool via the junction is condensed; the mass and energy exchange at the pool surface is calculated by the non-equilibrium zone model; the non-condensable gases entering the water are assumed to reach water temperature and are further released to the atmosphere above the water pool [12].

A particular attention has been devoted to the PC heat structures modelling to assess the impact of the Jet Impingement (JI), i.e. the effect of the injected water directly hitting the PC lateral hot wall. As a code user

strategy, the PC lateral wall has been artificially split into two different structures: the first one is modelled as a vertical lateral wall (as in the actual facility), while the second one has been defined as a floor horizontal structure, which can directly exchange heat with the water phase collected on the floor of the PC. Therefore, the code can better predict the direct heat exchange of the liquid injected into the PC with part of the lateral cylindrical wall of the chamber, and be able to accurately simulate the pressure behavior. A sensitivity analysis has been performed to determine the dimension of the floor horizontal structure to accurately predict the PC pressure peak. As a result of this study, half of the lateral surface of the PC cylindrical wall has been considered for the floor horizontal structure.

4 *Reference calculation results*

4.1 Pre-injection (PhW0)

A pre injection phase simulation has been carried out in order to reach the specific conditions of the test before the SOT. Table 2 shows the values of the initial conditions obtained by the ASTEC code against the experimental data at the SOT (t = 10 s).

Table 2: Comparison of experimental and calculated initial conditions

Parameter	Experimental data	Calculated data	Relative error
PC pressure	1000 Pa	1002 Pa	0.2 %
VV pressure	1000 Pa	1002 Pa	0.2 %
ST pressure	4000 Pa	4008 Pa	0.2 %
PC temperature	503.45 K	505.16 K	0.2 %
VV temperature	503.75 K	504.18 K	0.2 %
ST temperature	294.75 K	293.24 K	0.3 %
ST water level	61.6 %	61.4 %	0.3 %

In order to set the initial conditions for the ST, the tank has been assumed in thermal equilibrium with the external environment. The ST gas initial pressure is the sum of the steam saturation pressure and air partial pressure.

4.2 Transient analysis

The SOT is considered to take place at t = 10 s (start of PhW1). The calculated PC, VV and ST pressures, the PC liquid and gas temperatures and the ST water level are compared to the experimental data in Fig. 2, 3 and 5, with the four PhWs identified by dashed vertical lines. In Fig. 4 the liquid water mass in the PC is reported.

4.2.1 PhW1

The water injection in the PC starts at 10 s, which sets the beginning of PhW1. The flashing of the pressurized water in the low-pressure environment, enhanced by the contact with the PC hot walls, results in the production of superheated steam, determining a sudden pressure increase in the PC (Fig. 2, left) and in the connected VV (Fig. 2, right). The rate of pressurization of the PC and the peak of pressure reached are key factors in terms of safety of the system and are relevant for the evolution of the following transient sequence.

When the pressure in the PC reaches 0.15 MPa the MV opens, starting the steam discharge into the ST. From this point the pressure evolution of the system is governed by two counteracting phenomena: the liquid flashing, which tends to raise the PC and VV pressure; the pressure suppression action of the ST [9]. Initially, the pressure suppression in the ST has a lower impact and the PC and VV pressure continue to increase. Then, a change of slope in the PC and VV pressure can be observed from 13.5 s: the ST action becomes more effective due to the increasing pressure difference between the VV and ST. This pressurization phase is qualitatively and quantitatively well predicted by the code, as can be observed in Fig 2: a pressure peak of 0.465 MPa is reached in the PC at about 23 s for the experimental data, and of 0.453 MPa for the ASTEC simulation, with less than 2 s delay. After the peak the experimental PC and VV pressures slightly reduce during the remaining part of PhW1 (of the injection): at this point the ST effect has a higher weight than the pressurization one. This behavior is well predicted by the code simulation in which a slightly steeper reduction is predicted.

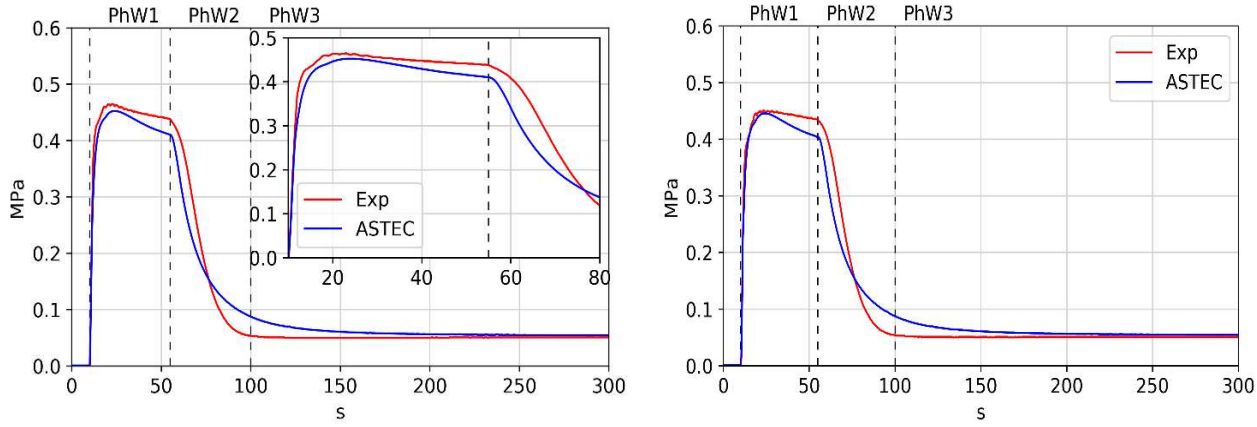

Fig. 2. PC (left) and VV (right) pressure for experimental data and ASTEC calculation

Since the code distinguishes between liquid and gas temperatures in the same zone, the two calculated PC temperatures have been reported in separated plot in Fig. 3. The calculated gas temperature is reported against the experimental data of a high elevation thermocouple (which is assumed to measure the gas phase temperature in PC), in Fig. 3 (left); the liquid calculated temperature is reported against a low elevation thermocouple (assumed to measure the liquid phase temperature on the bottom of PC), in Fig 3 (right). At the very beginning of the injection, the entrance of colder (in comparison to the initial PC wall temperature, in Table 1) pressurized water into the PC leads to a sudden drop of the experimental gas and liquid temperature, whose value moves from the initial condition (Table 1) to the saturation value at the PC pressure (Fig. 3). After the initial drop, following the saturation, the PC temperatures rise with the pressure, reaching a plateau corresponding to the saturation at around 0.45 MPa. This behavior is well predicted for the calculated liquid temperature, which reaches the saturation level as expected (Fig. 3, right). The gas-phase calculated temperature features a first heat-up, probably due to the fast gas compression, moving later to the saturation temperature which is the temperature at which the vapor is produced by the injected water flashing (Fig. 3, left).

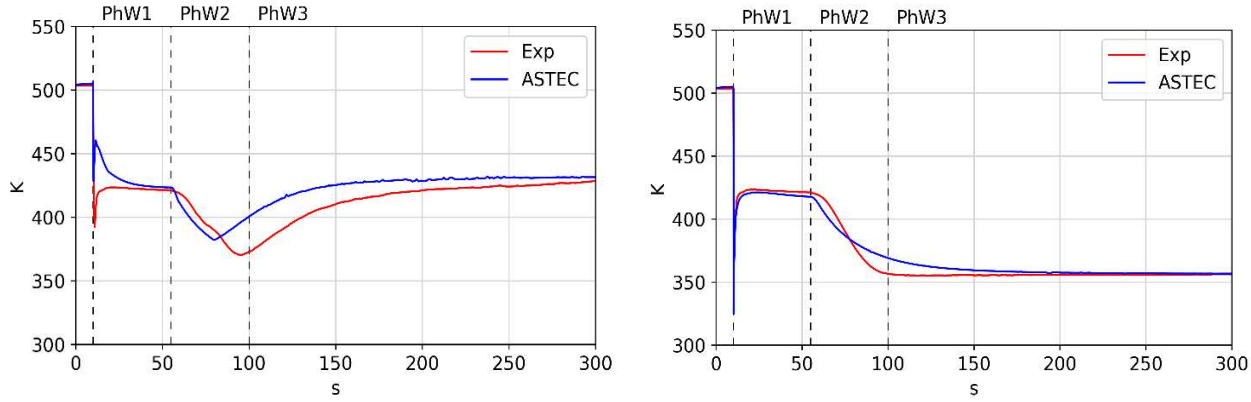

Fig. 3. PC gas-phase temperature (left) and PC liquid-phase temperature (right), ASTEC calculation against experimental results.

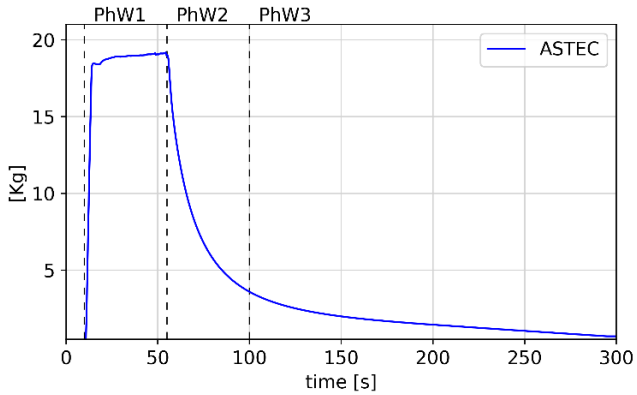

Fig. 4. calculated liquid mass in the PC.

The liquid water mass in the PC has been reported in Fig. 4. During PhW1 the code calculation predicts the condensation of steam in the PC zone (which includes the SD), as was visually observed in the experiment [3]. Part of the condensed water flows to the ST and, as can be seen in Fig. 5 (right), the ST water level is well predicted by the simulation.

According to the experimental data, in PhW1 the ST pressure increases with an almost constant rate until it reaches 0.04 MPa (Fig 5, left). The code, however, predicts a sharp pressure increase, reaching a peak of about 0.1 MPa, suddenly dropping to the expected value in the following phase. The different behavior can be attributed to the flashing of the pressurized liquid water coming from the VV into the ST; in fact, the INSERTION model used for the injection of gases into a pool (as mentioned in the §3.2) models only the steam and gas transfer. On the contrary, liquids cannot be injected directly into the sump but they end up into the gaseous phase, causing the flashing of the liquid itself.

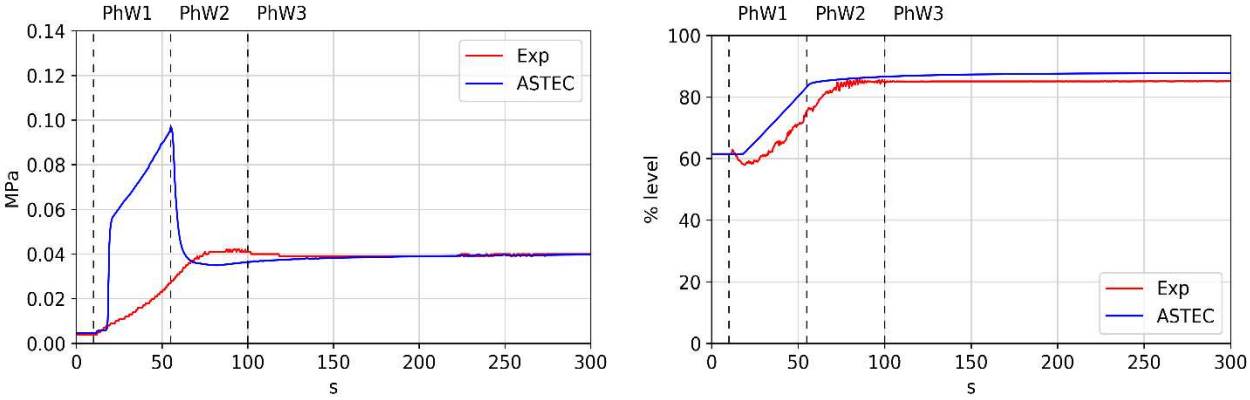

Fig. 5. ST pressure (left) and ST water level (right), for ASTEC calculation and experimental data.

4.2.3 PhW2

PhW2 begins with the end of the water injection in the PC at 55 s and is characterized by the PC and VV depressurization: the pressure in the PC and in the VV drops to about 0.05 MPa at the end of the phase (100 s of transient), as shown in Fig 2, since the MV is still open and water is continuously discharged into the ST. The calculated PC and VV pressures follow well the experimental depressurization behavior with a slightly different slope: the simulation reaches almost the same final value of pressure with a delay of 50 s (Fig. 2).

The liquid in the PC remains at saturation during the depressurization and its temperature decreases with the pressure in the chamber; this behavior is well predicted by the code (Fig. 3, right). Also the gas experimental temperature drops during this phase until, at the end of the depressurization, it rises again due to the superheating of the steam in contact with the upper hot walls of the PC [9]. The trend change of the gas temperature is anticipated by 20 s in the calculation with respect to the experimental behavior, probably due to a higher heat exchange with the walls (Fig. 3, left). The ST experimental pressure keeps rising due to the continuous water flow through the MV and then stabilizes at 0.04 MPa after about 85 s of transient (Fig 5, left). As soon as the PC injection stops, ASTEC compensates the ST overpressure, by dropping the pressure values slightly below 0.04 MPa; then the calculated pressure slowly increases until it approaches the experimental value, at about 0.04 MPa.

4.2.4 PhW3

During PhW3 (from 100 s to 300 s) the system reaches the final test conditions: the PC and VV pressures are almost constant at about 0.05 MPa and the ST pressure is constant too and close to 0.04 MPa (Fig. 2 and Fig. 5 left). The gas temperature in the PC, after the depressurization of PhW2, rises to about 425 K, in thermal equilibrium with the final PC walls temperature (Fig. 3, left). The experimental liquid temperature in the PC remains stable at the saturation value and at the end of the test the liquid water is still boiling (Fig 3 right). The PC and VV calculated pressures reach the expected final values with a delay due to the different slope of the depressurization. The pressure and temperature final conditions reached by the code at the end of the test well predict the final experiment values.

4.2.5 Relevant Thermal Hydraulic Aspects

A summary of the Relevant Thermal-Hydraulic Aspects (RTAs) of the experiment occurring in each PhW are compared with the ASTEC results in Table 3. All the phenomena are qualitatively predicted by the code in the correct PhW. Small quantitative differences in timing and values of the computed RTAs are present; the most important quantitative discrepancy is related to the ST pressure behavior (value and timing of the maximum) during PhW1-2.

Table 3: Experimental and calculated RTAs in characterizing the sequence

PhW	Time	Expected RTA	ASTEC RTA
0	0–10 s	-	-
1	10–55 s	• Beginning of water injection (at 10 s) • Opening of the MV (at 12 s) • PC maximum pressure: 0.465 MPa (at 23 s) • End of water injection (at 55 s)	• Beginning of water injection (at 10 s) • Opening of the MV (at 11.5 s) • PC maximum pressure: 0.464 MPa (at 24.5 s) • End of water injection (at 55 s)
2	55–100 s	• Maximum pressure in the ST: 0.042 MPa (at 87 s) • Onset of steam superheating (at 100 s)	• Maximum pressure in the ST: 0.095 MPa (at 57 s) • Onset of steam superheating (at 80 s)
3	100–300 s	• Final pressure in the PC: 0.051 MPa • Final pressure in the ST: 0.040 MPa • Final gas temperature in the PC: 427 K • Final liquid temperature in the PC: 356 K	• Final pressure in the PC: 0.052 MPa • Final pressure in the ST: 0.039 MPa • Final gas temperature in the PC: 432 K • Final liquid temperature in the PC: 357 K

5. Uncertainty Analysis

5.1 UA method adopted

Even though best estimate thermal-hydraulic computer codes have reached a high level of maturity, it should be considered that some uncertainties are unavoidably present due to models, correlations, code input-deck data, etc. These input uncertainties are propagated through the calculation and affect the results of the simulation [13]. In general, the sources of uncertainty can be divided into [14]: code uncertainty (e.g. approximation in the equations, models and correlations); representation uncertainty (nodalization effect); scaling (codes are in general validated against scaled down facilities); plant uncertainty (e.g. initial and boundary conditions); user effect. The execution of an UA has a great importance for the characterization of the uncertainty affecting computer code calculations and several methodologies have been developed in the past to perform UAs [14]. Among these methodologies, the probabilistic propagation of input uncertainties [15] is particularly suitable for code simulation applications and has been selected for the present work, as in [9]. The method is based on the random sampling of different values of the selected input uncertain parameters. The set of sampled values is used for running several code calculations, in which all the uncertain input parameters are sampled based on their own Probability Density Function (PDF) [16]. From a statistical analysis

of the collected calculations results, the relationship between the input uncertain parameters and the output FOMs can be characterized. Some uncertainty tools are available based on this methodology: the present UA employs the RAVEN tool [8], developed by Idaho National Laboratory.

5.2 RAVEN tool and coupling methodology adopted

RAVEN [8][17] is a flexible and multi-purpose uncertainty quantification, regression analysis, probabilistic risk assessment, data analysis and model optimization framework. Depending on the tasks to be accomplished and on the probabilistic characterization of the problem, RAVEN is able to study the system perturbation in response to randomly sampled parameters. The system is modeled by third party software (e.g., RELAP5-3D, MAAP5, BISON, etc.) accessible to RAVEN either directly (software coupling) or indirectly (via input/output files). The results data of the calculations generated by the sampling process are analyzed using classical statistical and more advanced data mining approaches. RAVEN also manages the parallel dispatching (both on desktop/workstation and large High Performance Computing machines) of the software representing the physical model. RAVEN heavily relies on artificial intelligence algorithms to construct surrogate models of complex physical systems in order to perform uncertainty quantification, reliability analysis (limit state surface) and parametric studies.
For all the codes currently supported (e.g. RELAP-7, RELAP5-3D, BISON, MELCOR, etc.), the coupling is performed through a Python interface that interprets the inputs coming from RAVEN, translates them into the input of the driven code and gather the physical model output. Since RAVEN is an open source software, the procedure for coupling it with a new physical model code allows the creation of a new Python interface that is going to be embedded at runtime [17].
In the framework of the current work, a Python interface has been developed for the ASTEC-RAVEN coupling. An appropriately modified input file of the ASTEC model of the reference calculation needs also to be provided for the coupling. The RAVEN input file consists in an eXtensible Markup Language (XML) file containing all the UA calculation options [17]:

- The uncertain input parameters, their ranges and PDFs type;
- The sampling method (e.g. Monte Carlo, Latin Hypercube, etc.) and the desired number of calculations *N*;
- The communication options with the HPC infrastructure (parallel protocol, nodes address file, number of code calculations to be run in parallel);
- The output FOMs selected for the UA and the desired statistical analyses to be performed.

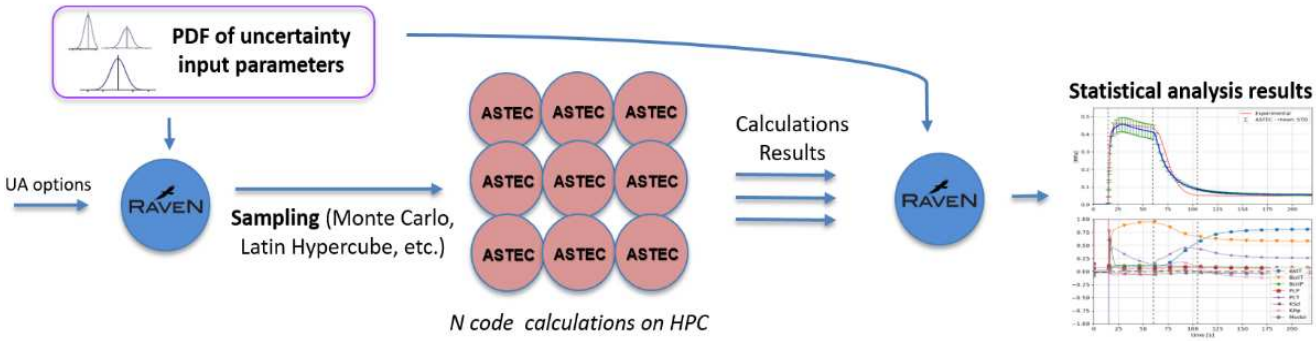

Fig. 6 ASTEC – RAVEN coupling workflow for uncertainty analysis.

Fig. 6 presents the ASTEC-RAVEN coupling workflow for the UA method applied. Starting from the selected uncertain input parameters (together with their range and PDF) and the UA options (total number of calculations *N*, sampling methods, etc.), RAVEN samples the input parameters on the base of their PDFs and creates a set of *N* ASTEC inputs. Based on Wilks studies [18][19], the minimum number of code runs *n*, has been determined. The total number of calculation $N \geq n$, has to be chosen by considering also the time required for each single calculation and the available computational power (number of CPUs running in parallel in the present case). The set of *N* ASTEC calculations is then performed and the set of results is collected by RAVEN. By reprocessing the results data-set and the sampled values of the input uncertain parameters, the uncertainty tool is able to perform the statistical analysis. In addition to the basic statistical parameters (mean, percentiles, Standard Deviation, etc.), RAVEN can compute several response correlation and regression coefficients

(Pearson, sensitivity, normalized sensitivity, etc.). In this study the Pearson and the Spearman correlation coefficients [9] have been employed as indicators to evaluate the correlation between the input uncertain parameters and the FOM. The Pearson coefficient is a measure of the degree of linear correlation between two variables and it ranges between -1 and +1: if the value of the coefficient is lower than zero, the two variables are negatively correlated (an increment of x leads to a reduction in y); if the coefficient is equal to zero, there is no linear correlation between the two variables; if it is greater than zero, the linear correlation is positive (an increment of x leads to an increment of y). The Spearman coefficient is a rank correlation coefficient and it is calculated by ranking the data in ascending order instead of using the actual data values. Like Pearson, the Spearman coefficient ranges between -1 and +1 and it measures the monotonic relation between the two variables: if two variables are monotonically related without repetitions the Spearman coefficient is exactly -1 or +1, depending on whether the variable are increasing in the same or in the opposite direction [9]. The Spearman coefficient was calculated with the support of the SciPy library of Python [20].

5.3 Implementation on CRESCO HPC

The CRESCO6 cluster [10] architecture provides a total of 434 nodes and 48 CPU per node, for a total of 20832 cores connected by a 100 Gb/s Intel Omni-Path-based broadband and low latency network. The procedure for running multicore calculations is the submission of a "batch job" on a specific queue, specifying the number of cores requested. Once the CPUs are available, the system assigns one or more nodes on which are located the requested cores to run the calculation. RAVEN is capable of running MPI parallel processes and read the file containing the assigned nodes addresses provided by CRESCO. Each ASTEC calculation is a serial process running on one of the available cores of the CRESCO dual-CPU nodes. In our application several batch jobs demanding 48 parallel running cores (limit of the selected queue) have been submitted for a total of 200 calculations. In order to run ASTEC on an HPC environment, a license server is required, so that it manages all the concurring executions up to the limits of the license.

5.4 Assumptions adopted in the UA

Following the general approach described in [9], the selection of the input uncertain parameters for the UA depends: on the available data concerning the facility, its component, geometry and features; on the initial and boundary conditions of the experiments; on the control logic of the experiment. Once the parameters have been selected, in order to characterize the related uncertainties for each of them it should be identified:

1) The reference value;
2) The range of variation of the parameter;
3) The associated PDF.

In particular, the definition of the PDF is a challenging task since universal guidelines are not available. If there is no evidence that a particular PDF should be chosen, the uniform distribution can be used. in fact, at a fixed range, it assigns the same probability to all the values in the range of variation of the parameter; however this can lead to a results spreading larger than the one obtained with the use of peaked type distributions [9][21].

In Table 4 the uncertain input parameters used are listed with their range and PDF. Following the methodology adopted in [9], the PDF and the range of variation for some parameters (marked with an * in Table 4) have been derived from an analysis of ICE performed with RELAP5 code and SUSA tool for the Wendelstein 7-X (W7-X) Stellarator in Germany [22]. For the remaining input parameters, since the authors have no information to characterize the PDFs and the related ranges, the authors decided to adopt a large range [-100%; +100%] and a uniform distribution. As a hypothesis, the ST has been assumed in thermal equilibrium with the external environment at the SOT. Hence, the ST initial temperature and the external temperature have the same distribution and have been sampled together as a single uncertain parameter. The Monte Carlo sampling has been selected. The PC pressure has been chosen as FOM since it would be the most relevant parameter in case of a safety analysis.

Considering the large computational power available from the CRESCO HPC, a probability content of 98% and a confidence level of 98% has been selected for the analyses. Based on the Wilks' formula, having only one FOM, for the one-sided statistical tolerance limits the number of calculation required to have a probability content of 98% and a confidence level of 98% is n = 194. Therefore, a total of N = 200 calculations have been selected for the UA.

Table 4: Uncertain parameters selected for the analysis

Parameter	Range of variation	PDF type
ST initial temperature and external temperature (extT)*	[-5%; +5%]	Uniform
Boiler temperature (BoilT)*	[-3%; +3%]	Normal
Boiler pressure (BoilP)*	[-3%; +3%]	Normal
PC, SD, VV initial pressure (PcP)*	[-20%; +20%]	Normal
PC, SD, VV initial temperature (PcT)*	[-3%; +3%]	Uniform
Minor loss coefficient at the SD slits (KSd)	[-100%; +100%]	Uniform
Minor loss coefficient at the MV (KRp)	[-100%; +100%]	Uniform
MV opening delay (Mvdel)[1]	[-100%; +100%]	Uniform

[1]The MV opening delay is the delay time considered for the start of the MV opening, with respect to the reaching of the pressure sent-point in the PC.

5.5 UA results

5.5.1 Results dispersion

All the 200 runs have been successfully completed.

In order to characterize the results dispersion band against the experimental data, in Fig. 7 the PC calculated pressure has been plotted for all the 200 cases, along with the experimental pressure.

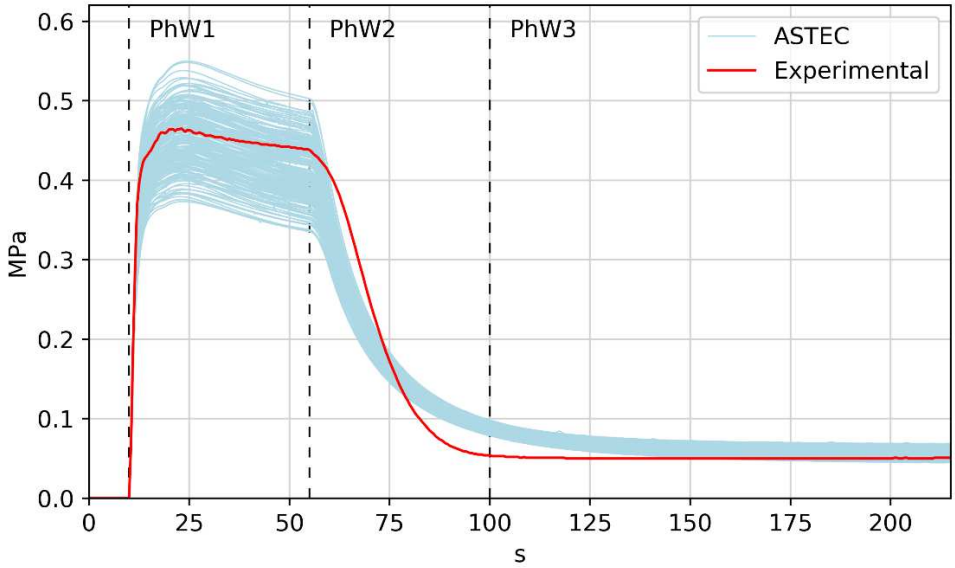

Fig. 7 Dispersion of the calculated data of the PC pressure vs experimental data

In Fig. 8 the mean value and the Standard Deviation (STD) of the calculated PC result have been reported against the experimental data.

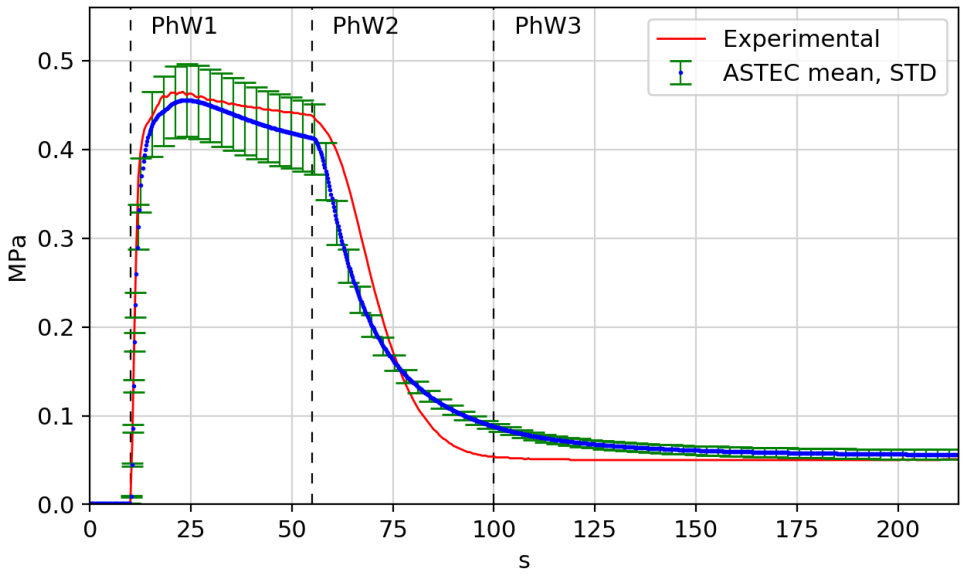

Fig. 8 Mean and STD of the calculated PC pressure vs experimental data

During PhW0 (0 – 10 s), the PC pressure dispersion coincides with the uncertainty of the input parameter "initial PC pressure", sampled as uncertain initial condition in the calculations.

Fig. 7 shows that in PhW1 (10 – 55 s) the results dispersion band width increases as the pressure builds up until it reaches its maximum value; then it stays almost constant for the rest of the PhW. The experimental trend is always within the results dispersion band and it is close to the mean value of the simulations. The dispersion band width in PhW1 features a value of around 0.2 MPa and the maximum calculated value is of 0.55 MPa.

Along PhW2 (55 – 100 s) the FOM results dispersion band width reduces during the depressurization. In this window the experimental pressure is not entirely included in the dispersion band due to the different decreasing pressure slopes. Since the calculated slope seems to be similar in all the calculations, as can be inferred by looking at Fig. 7, the slope discrepancy with respect to the experimental curve cannot be attributed to any of the uncertain parameters.

.

In the last PhW (after 100 s) the results dispersion band width remains narrow (around 0.04 MPa) and once the calculated values reach the final steady conditions the experimental pressure falls within the dispersion band up to the end of the calculation.

5.5.2 Response correlations results

The values of the Pearson and Spearman response correlation coefficients related to the PC pressure and computed for the eight distributions are reported in Fig 9 and 10 along the evolution of the transient. The Pearson and the Spearman coefficients give respectively a measure of the linearity and of the monotonicity related to the correlation between each uncertain input parameter and the chosen FOM. This allows to understand how the relationship between the selected uncertain input parameters and the chosen FOM varies during the transient in the different PhWs considered. As explained in [9] and in [23], if the absolute value of the correlation coefficient is higher than 0.5, the correlation can be classified as significant; between 0.2 and 0.5 the correlation it can be considered moderate; otherwise the correlation is low.

In the results of this application it can be observed that the two response correlation coefficients show very similar trends.

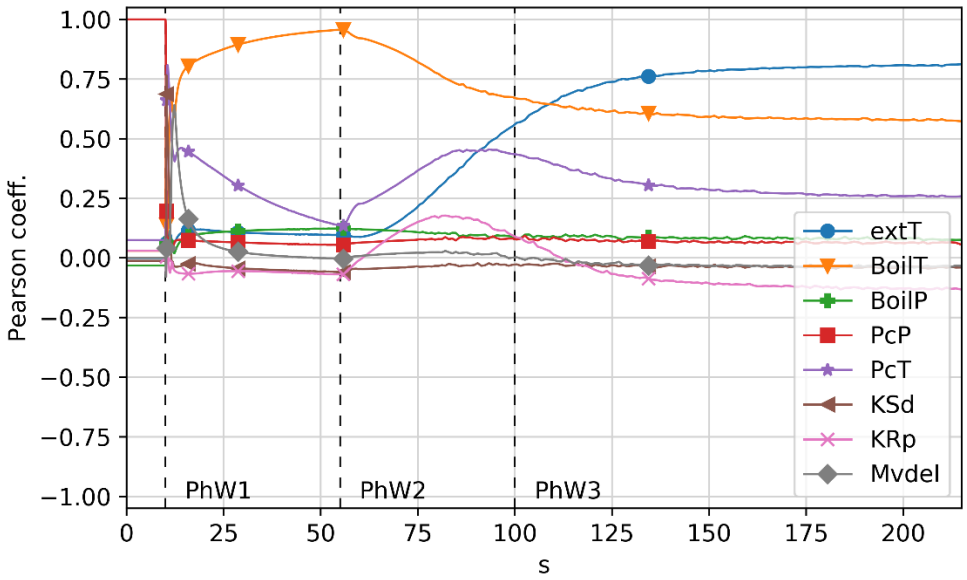

Fig. 9 Pearson correlation coefficient related to the PC pressure along the transient.

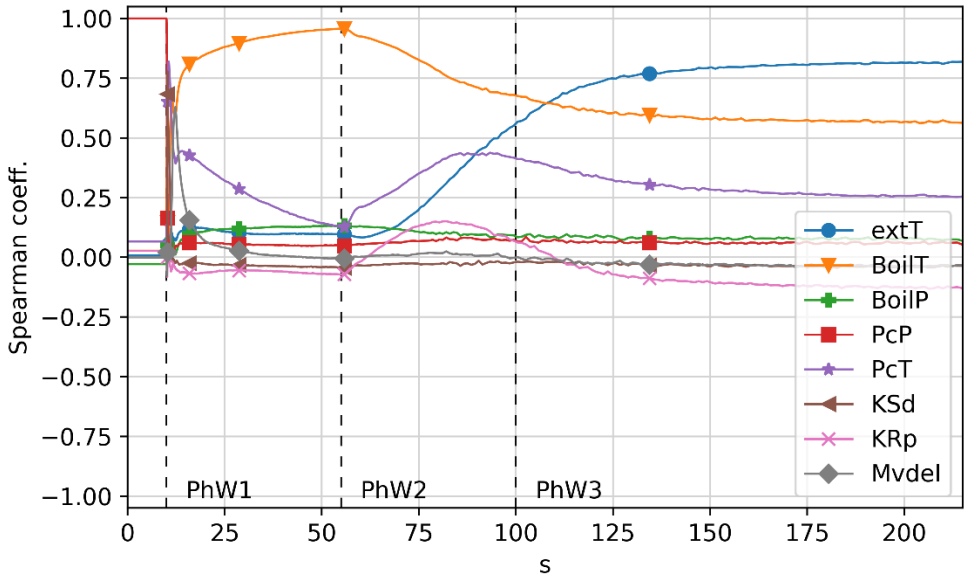

Fig. 10 Spearman correlation coefficient related to the PC pressure along the transient.

In PhW0 (0 – 10 s) the values of the FOM coincide with the PC initial pressure (PcP) and hence, as expected, the value of the two correlation coefficients related to this parameter is one.

As soon as the water injection begins in PhW1 (10 – 55 s), the Pearson and Spearman coefficients of the PC initial pressure become negligible, while the boiler temperature coefficients smoothly increase up to reach a maximum value of 0.98, at the end of PhW1. Thus, the injection temperature has a significant correlation with the FOM. And this is consistent with the energy inserted with the water injected, whose enthalpy depends mainly on the fluid temperature. The plots show also that the SD slits loss coefficient (KSd) and the MV opening delay (Mvdel) display a significant correlation with the FOM only at the moment of the valve opening, with two narrow peaks. This can be explained as a longer valve opening delay and a higher pressure losses reduce the pressure suppression action of the ST. Finally, the PC structures initial temperature Pearson and Spearman coefficients (PcT) feature a strong peak (up to 0.8) at the very beginning of the injection, proving the significant relationship occurring in the first seconds of pressurization due to the water-walls direct contact. A lower correlation with the FOM is observed during the following part of PhW1, when the walls in contact with liquid water have been partially cooled down to the water temperature. All the other input uncertain parameters show a weak correlation to the PC pressure in this PhW.

In PhW2 (55 – 100 s) the boiler temperature coefficients start to decrease since after the injection end its correlation with the PC pressure is only due to the long term effect of the previous PhW. On the contrary, once

terminated the injection, the Spearman and Pearson coefficients of both the ST initial temperature (and external temperature) and of the PC initial temperature increase: the extT increases since with an initially hotter ST pool the suppression effect is lower, leading to higher PC pressure; while the increase of the PcT is due to the heat exchange between the PC walls and the steam that, once the injection has ended, has probably a higher phenomenological weight.

In the final phase (after 100 s), the boiler temperature correlation coefficients keep decreasing, yet remaining significant at around 0.6 and therefore showing a long term effect of this parameter until the end of the test. The ST initial and external temperatures reach significant positive correlation coefficients, higher than 0.8. This is probably due to the influence of the external temperature, which causes a slower cooling and therefore a slower depressurization.

Based on the discussed results, it would seem appropriate to reduce the uncertainty of the inputs that show the highest correlation with the FOM in PhW1 for two main reasons: first, because it is the phase in which the largest results dispersion is observed; secondly because in PhW1 the PC pressure reaches its maximum values, and this determines the most challenging safety conditions. Therefore, the analysis made on the Pearson and Spearman coefficients in Fig. 9 and 10 respectively, suggests that the input uncertain parameters having a major correlation with the selected FOM, during the most challenging safety conditions are: the boiler injection temperature, the PC initial temperature, the minor loss coefficient at the SD slits and the MV opening delay.

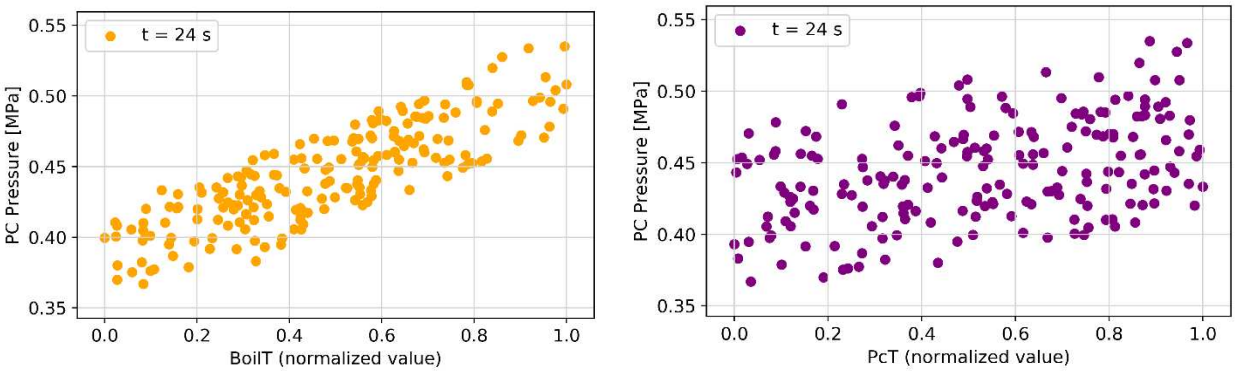

Fig. 11 PC pressure for each input value of the boiler injection temperature (left) and of the PC initial temperature (right), at t = 24 s.

Fig. 11 shows two scatter plots visualizing the values of the PC pressure for each input value of the injection temperature (Fig. 11, left) and of the PC initial temperature (Fig. 11, right) at 24 s (all the uncertainty calculations reach the PC maximum pressure around this time). A positive correlation can be observed for both the parameters, as expected from the Pearson and Spearman coefficients. All the other input uncertain parameters feature no observable correlation in the respective scatter plot at this specific time.

6. Conclusions

CPA module of the ASTEC V2 severe accident code has been adopted for the simulation of a test conducted in the ICE facility. The experimental results of the main thermal-hydraulic parameters have been compared to the code results to characterize the ASTEC capability to predict the phenomenology of an ICE event in a fusion reactor. The ASTEC model has been described and discussed in the present paper. A deterministic simulation of Case 4 of the ICE experimental campaign has been performed and the results of the study have been analyzed against the experimental data. The comparison proves the capability of the ASTEC code, and in particular of its CPA module, to qualitatively simulate all the main thermal-hydraulic phenomena characterizing the ICE-type accidents in fusion reactors. The phenomena of water flashing in an under vacuum environment and the following pressurization seems to be well predicted by the code.

The second part of the paper is dedicated to the description of the methodology adopted in the UA performed on the selected test simulation. The uncertainty quantification method applied through the RAVEN-ASTEC coupling and the implementation on the CRESCO HPC architecture have been described in the paper. The aim of the work is not to provide an exhaustive uncertainty study, but to give some insights characterizing the dispersion of the results against the available experimental data. Moreover, the analysis provides a first

example application of the RAVEN-ASTEC codes coupling for uncertainty quantification with the use of an HPC.

In the UA study the PC pressure has been assumed as FOM since it is the main thermal-hydraulic parameter to be considered in terms of safety. The statistical analysis performed aims at characterizing the propagation of the input uncertainty to the FOM along the transient. The study of the associated Pearson and Spearman coefficients provides useful insights regarding the correlation between the selected uncertain input parameters and the FOM.

The results of the UA suggest that the phase of the transient in which the FOM is mostly affected by uncertainty is the injection phase (PhW1). The study made on the Pearson and the Spearman coefficients suggests that the input uncertain parameters having a major correlation with the selected FOM during the most challenging safety conditions are: the boiler injection temperature, the PC initial temperature, the loss coefficient at the SD slits and the MV opening delay. Efforts should be concentrated in improving their characterization and reducing the associated uncertainty.

Future activities could concern the improvement of the ICE facility nodalization, with the aim of studying whether a finer nodalization results in reduced spread of the uncertainty to the FOM and assessing its effect in the uncertainty propagation.

Acknowledgments

The authors gratefully acknowledge the valuable support provided by IRSN in the preparation of the work described in the paper.

The computing resources and the related technical support used for this work have been provided by CRESCO/ENEAGRID High Performance Computing infrastructure and its staff [10]. CRESCO/ENEAGRID High Performance Computing infrastructure is funded by ENEA, the Italian National Agency for New Technologies, Energy and Sustainable Economic Development and by Italian and European research programs, see http://www.cresco.enea.it/english for information.

References

[1] T. Pinna, D. Carloni, A. Carpignano, S. Ciattaglia, J. Johnston, M.T. Porfiri, L. Savoldi, N. Taylor, G. Sobrero, A.C. Uggenti, M. Vaisnoras, R. Zanino, Identification of accident sequences for the DEMO plant, Fusion Eng. Des. 124 (2017) 1277-1280

[2] K. Takase, H. Akimoto, L.N. Topilski, Results of two-phase flow experiments with an integrated Ingress-of-Coolant Event (ICE) test facility for ITER safety, Fusion Eng. Des. 54 (2001) 593-603

[3] K. Takase, H. Akimoto, Experimental verification of effectiveness of integrated pressure suppression systems in fusion reactors during in-vessel loss of coolant events, Nucl. Fusion 41 (2001) 1873-1883

[4] IAEA, ITER-FEAT Outline design report, https://www-pub.iaea.org/MTCD/Publications/PDF/ITER-EDA-DS-18.pdf (2001)

[5] T. Marshall, M.T. Porfiri, L. Topilski, B. Merril, Fusion safety codes: international modeling with MELCOR and ATHENA–INTRA, Fusion Eng. Des. 63–64 (2002) 243–249

[6] T. Kačegavičius, E. Urbonavičius, Modelling of ingress of coolant event into vacuum experiments with ASTEC code, J. Fusion Energy 34 (2014) 320–325

[7] P. Chatelard, S. Belon, et al., "Main modelling features of the ASTEC V2.1 major revision", Annals of Nucl. Energy, 93, pp. 83-93, (2016)

[8] A. Alfonsi, C. Rabiti, D. Mandelli, J. Cogliati, C. Wang, P. W. Talbot, D. P. Maljovec, C. Smith, RAVEN Theory Manual and User Guide. INL/EXT-16-38178. (2017)

[9] A. Bersano, F. Mascari, M.T. Porfiri, P. Maccari, C. Bertani, "Ingress of Coolant Event simulation with TRACE code with accuracy evaluation and coupled DAKOTA Uncertainty Analysis.", Fusion Engineering and Design 159, 111944 (2020)

[10] F. Iannone et al., CRESCO ENEA HPC clusters: a working example of a multifabric GPFS Spectrum Scale layout, International Conference on High Performance Computing & Simulation (HPCS), Dublin, Ireland, 2019, pp. 1051-1052, doi: 10.1109/HPCS48598.2019.9188135, (2019).

[11] G. Caruso, M.T. Porfiri, CONSEN validation against ICE and EVITA Experimental campaign 2000 Pre-test calculations, FUS-TN-SA-SE-R-09 (2000)
[12] N. Reinke, W. Klein-Hessling, and B. Schwinges, CPA Module of ASTEC Programme Reference Manual. ASTECV2/DOC/15-03 DRAFT Version Rev 1, Gesellschaft fur Anlagen-und Reaktorsicherheit (Germany) and Institut de Radioprotection et de Surete Nucleaire (France), (2015)
[13] F. Mascari, H. Nakamura, K. Umminger, F. De Rosa, F. D'Auria, Scaling issues for the experimental characterization of reactor coolant system in Integral Test Facilities and role of system code as extrapolation tool, Proceedings of 16th International Topical Meeting on Nuclear Reactor Thermal Hydraulics (NURETH-16), 6 (2015) 4921-4934
[14] IAEA International Atomic Energy Agency, Best Estimate Safety Analysis for Nuclear Power Plants: Uncertainty Evaluation, Safety Reports Series (2008)
[15] H. Glaeser, GRS Method for Uncertainty and Sensitivity Evaluation of Code Results and Applications, Sci. Technol. Nuc. Ins. (2008)
[16] A. Bersano, F. Mascari, Evaluation of a Double-Ended Guillotine LBLOCA Transient in a Generic Three-Loops PWR-900 with TRACE Code Coupled with DAKOTA Uncertainty Analysis, ATW - International Journal for Nuclear Power 11/12 (2019) 526-532
[17] C. Rabiti, A. Alfonsi, J. Cogliati, et al. Raven user manual. No. INL/EXT-15-34123 (Revision 6). Idaho National Lab.(INL), Idaho Falls, ID (United States), (2017)
[18] S.S. Wilks, Determination of sample sizes for setting tolerance limits, Ann. Math. Stat. 12(1) (1941) 91-96
[19] S.S. Wilks, Statistical prediction with special reference to the problem of tolerance limits, Ann. Math Stat. 13(4) (1942) 400-409
[20] P. Virtanen, R. Gommers, T. E. Oliphant, et al. SciPy 1.0: fundamental algorithms for scientific computing in Python. Nature methods, 17(3), 261-272, (2020)
[21] M.E. Stephens, B.W. Goodwin, T.H. Andres, Deriving parameter probability density functions, Reliab. Eng. Syst. Safe. 42 (1993) 271-291
[22] T. Kaliatka, E. Ušpuras, A. Kaliatka, D. Naujoks, Analysis of ingress of coolant accident in the vacuum vessel of the W7-X fusion experimental facility, EUROFUSION WPSAE-PR(16) 16324, (2016)
[23] K.A. Gamble, L.P. Swiler. Uncertainty quantification and sensitivity analysis applications to fuel performance modeling, SAND2016-4597C, (2020).

Abbreviations

FOM	Figure Of Merit
ICE	Ingress of Coolant Event
HPC	High Performance Computer
JAERI	Japan Atomic Energy Research Institute
JI	Jet Impingement
LOCA	Loss Of Coolant Accident
LWR	Light Water Reactor
MV	Magnetic Valve
PC	Plasma Chamber
PDF	Probability Density Function
PhW	Phenomenological Window
PSA	Probabilistic Safety Assessment
RP	Relief Pipe
RTA	Relevant Thermal-hydraulic Aspects
SA	Severe Accident
SD	Simulated Divertor
SOT	Start Of the Transient
ST	Suppression Tank
STD	Standard Deviation
UA	Uncertainty Analysis
VV	Vacuum Vessel
XML	eXtensible Markup Language